Ensemble Forecast of a Typhoon Flood Event

BRIAN P. MACKEY AND T. N. KRISHNAMURTI

Department of Meteorology, The Florida State University, Tallahassee, Florida

(Manuscript received 9 September 1999, in final form 2 February 2001)

ABSTRACT

A high-resolution nested regional spectral model and an ensemble prediction system are combined to forecast the track, intensity, and flooding precipitation arising from Typhoon Winnie of August 1997, which eventually reached supertyphoon status. The prediction of floods is operationally challenging since rainfall distributions can have a high degree of spatial and temporal variability. Rare event probabilities, however, can be estimated more readily via ensemble forecasting. This technique is used to evaluate a typhoon flood event in which rainfall amounts greater than 200 mm led to landslides and major flooding of crops. Seven-member ensembles were generated using an EOF-based technique. An experiment was conducted with a regional model resolution of 0.5° latitude. A Mercator transform grid with a grid mesh size of approximately 55 km in the east–west and 48 km in the north–south was employed. The results indicated very accurate track and intensity forecasts for both the control and ensemble mean. Track position errors remained below 150 km through 72 h, while intensity errors were approximately 5 m s^{-1} at landfall. Qualitatively, the overall 5-day precipitation patterns appeared realistic and compared favorably with the observed data, while, quantitatively, the correlation coefficient was near 0.6. For stations near and north of where Winnie made landfall, ensemble-based predictions performed well. While the ensemble mean often underestimated the heaviest rainfall totals by approximately 25%–50%, the maximum values within the ensemble spread either exceeded or came within 10%–15% of the station totals. Finally, in a related experiment the horizontal resolution was increased to 0.25° latitude. Even though more precipitation was produced, especially in northeastern China, the ensemble mean was similar to the 0.5° latitude simulation.

1. Introduction

Tropical cyclones are among the world's most serious threats to life and property with the primary dangers being storm surges, strong winds, and flooding due to heavy rainfall. According to a World Meteorological Organization (WMO) study (De and Joshi 1998), tropical cyclones rank second among all natural disasters in loss of life behind drought. As a result, nearly 900 000 deaths occurred around the world from 1967 to 1991. Typhoons in the western North Pacific Ocean basin annually cause more than $4 billion in total losses based on estimates by the Asian and Pacific Typhoon Committee of the WMO (Chen 1995).

In this study, the focus will be on the flooding rains resulting from the passage of Typhoon Winnie of August 1997, which seriously affected portions of Taiwan and eastern China. Intense precipitation in tropical cyclones can be traced back to an enhanced hydrological cycle due to warm sea surface temperatures, sustained high winds, and sea spray (Raj 1998). As a storm approaches land, flooding rains can occur within the core region, spiral bands, and even along inverted troughs to the north of the cyclone. These troughs are most pronounced in the western North Pacific basin and near the coast of China. In the case of Typhoon Winnie, heavy rains occurred in each of these areas. Moreover, coastal boundaries and mountainous terrain provide another important means for producing torrential rainfall and landslides. Over northern Taiwan, for instance, the hilly, steep terrain played a role in creating mudslides as Winnie passed by to the north. Finally, increased convergence along a coastline to the right of a storm (in the Northern Hemisphere) can occur because of blocking and frictional effects of a landmass (Chen 1995). In this case, the large landmass of China likely served to increase the convergence and heavy precipitation to the north of the typhoon's center.

In order to investigate this event, the Florida State University Nested Regional Spectral Model (FSUNRSM) (Cocke 1998) is employed, along with an empirical orthogonal function (EOF) perturbation method following Zhang (1997), to generate ensemble forecasts of the track, intensity, and precipitation. The regional model used here is designed to be compatible with the Florida State University Global Spectral Model (FSUGSM). Details about the models are available in the appendices.

Corresponding author address: Brian P. Mackey, Department of Meteorology, The Florida State University, 404 Love Building, Tallahassee, FL 32306-4520.
E-mail: mackey@met.fsu.edu

2. Ensemble forecast of floods

Ensemble forecasting takes into account the inherent uncertainty in the initial data fields as well as the model formulation of the atmosphere. This introduces a probabilistic aspect to the model forecasts as well as a significant challenge—to ensure that an ensemble includes the full range of possible initial states so that all potential forecasts can be considered. This is practically impossible to accomplish. Nevertheless, by sufficiently perturbing the initial conditions, a wide range of plausible forecasts is attainable. It can be shown that the best perturbations are those that (a) adequately sample the error probability distribution, and (b) give distinct, yet reasonable, outcomes. For example, if it is known a priori that two forecast results are quite similar, then it is unnecessary to run both cases.

The perturbation method employed in this study is based upon EOFs. An ensemble is generated specifically for tropical weather prediction (Zhang 1997; Zhang and Krishnamurti 1997, 1999). Other methods currently in use around the world are more suited for midlatitude prediction and therefore may not be adequate for tropical studies due to the differences in dynamics, physics, and causes and rates of perturbation growth. For instance, singular vectors (Buizza and Palmer 1995; Molteni et al. 1996) are predicated on linear dynamical instability and leave out physical processes. In addition, the breeding method (Toth and Kalnay 1997) determines perturbations for the entire globe, and it largely depends upon baroclinic instabilities over the midlatitudes.

The EOF-based ensemble technique examines only two of the most important tropical variables—temperature and wind—partly in order to keep computations at a minimum. A moisture parameter may also be utilized, however. As a first step, random temperature and wind perturbations with amplitudes comparable to forecast errors are added to the control analysis. Then, both the unperturbed (control) and the perturbed analyses are integrated for an optimal 36 h using the complete version of the FSUGSM with full physics. During this time, it is presupposed that only linear growth has occurred. From both forecasts, time series of difference fields of temperature and wind are constructed every 3 h beginning with hour 6 of the forecast. This ensures that random effects do not degrade the process. Next, scalar EOF analysis is performed on the temperature time series while a complex EOF technique is used for the wind series. Ultimately, the first three eigenvectors (modes) are added to and subtracted from the control analysis resulting in seven ensemble members, including the control. These first three modes are considered to be the fastest growing, and presumably, large portions of these modes will be projected onto the most dynamically unstable directions. Consequently, these resulting perturbation patterns should adequately sample the initial error probability distribution, and thus the perturbations can be deemed optimal. The initial perturbation amplitudes are scaled to approximate the 3-h forecast error, which is 3 m s^{-1} for the wind field and 0.6° K for the temperature field.

An ensemble forecast can easily provide much more information than a single, deterministic model run since each individual forecast within the ensemble suite can be assigned a probability of occurrence. Ensemble flood forecasts are especially beneficial as rainfall distributions may exhibit large variability on all time and space scales. Model-based precipitation errors can quickly become significant even over small areas. Ensembles are also useful tools in evaluating extreme or unusual weather events, such as floods. If an ensemble adequately samples all possible forecasts, then such an event is likely to be well predicted by the first moment, and an understanding of the uncertainty is possible from the second moment. Hence, it is obvious that probabilities of an extreme event can be estimated more readily via ensemble forecasting (Hamill and Colucci 1998).

Very few studies have addressed the use of ensemble NWP methods to forecast tropical cyclone–related floods. First, a successful prediction of a typhoon's heavy rain areas is based upon an accurate forecast of the typhoon's path, strength, and structure. In addition, air–sea interactions and moisture, temperature, and wind fields surrounding the typhoon must be accurately represented as well as boundary parameters, such as sea surface temperatures and topography. By using a proven high-resolution spectral model and an ensemble prediction system, a detailed case study of Typhoon Winnie is performed where the observed track and intensity is compared to that from a 5-day ensemble forecast. This study will focus on the rainfall and subsequent flooding caused by Winnie. By comparing station and satellite-derived precipitation data to the model ensemble, a qualitative assessment of the forecast skill is given. A final goal of this study is to examine what effect, if any, a higher-resolution regional forecast would have on the precipitation patterns and amounts.

In this research, the ensemble maps will attempt to convey useful probabilistic information to the user. An ensemble mean chart of the total precipitation is one such product. It is best to treat this type of map with caution, however, as some smoothing of the maximum rainfall is probable. The ensemble mean will tend to enhance characteristics that are similar to all members while giving little significance to their differences (Sivillo and Ahlquist 1997). Marked smoothing is especially noticeable if the rainfall probability distribution is bimodal, or doubly peaked in two separate areas. Often, a distribution such as this occurs when two distinct outcomes are possible. For instance, if it is in question whether or not a midlatitude trough will help to recurve a tropical cyclone, then a bimodal rainfall distribution may result.

Ensemble forecast information can also take the form of ''postage stamp'' maps where each member forecast is displayed on one page. Thus, one can quickly view

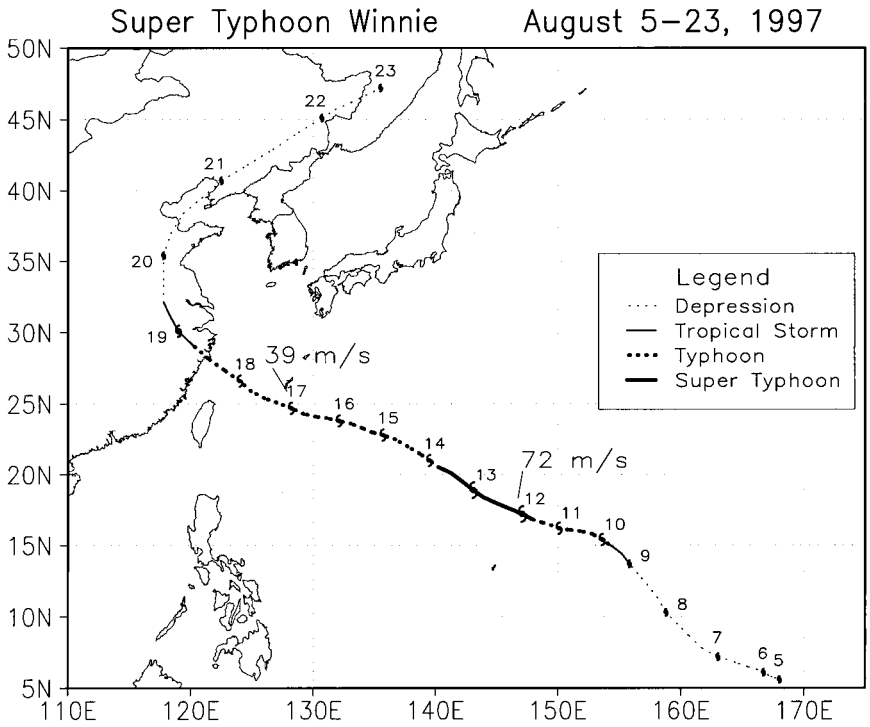

FIG. 1. Best (observed) track and intensity of Typhoon Winnie.

and assess the possible outcomes. Moreover, at certain key grid points time series of any variable can be created with error bars indicating the ensemble spread. Finally, probability distribution maps of precipitation, for example, can map out areas that have a high risk of torrential rains. In this manner, the user is presented with a numerical estimate of whether or not a certain rainfall threshold would be reached. Therefore, with an optimally perturbed ensemble forecast, one is likely to achieve a superior flood forecast and have a good sense of the qualitative and quantitative uncertainty.

3. Typhoon Winnie

Figure 1 shows the observed track for Typhoon Winnie as compiled by the Joint Typhoon Warning Center (JTWC). Typhoon Winnie originated from an area of low pressure in the monsoon trough near 170°E on 5 August 1997 over the open waters of the northwest Pacific Ocean. As it moved northwest, Winnie steadily intensified and reached typhoon strength on 10 August about 900 km east of Guam. Two days later Winnie gained supertyphoon status and peaked at an estimated 72 m s^{-1} (898 hPa) just after passing over the sparsely populated northern Mariana Islands.

While continuing on a west-northwest course, Winnie slowly weakened, but was still a major threat to eastern Asia. On 16 August as Winnie neared the island of Okinawa, an interesting transformation of the central core features took place. An outer rainband formed and then completely encircled the eye and eyewall of Winnie. With a diameter reaching approximately 350 km, this was one of the largest outer eyewall features ever observed (Lander 1999).

After passing Okinawa, Winnie was centered about 125 km northeast of Taiwan with an estimated intensity of approximately 39 m s^{-1} on 18 August. This was the closest point of approach to Taiwan, but since Winnie's wind and precipitation fields were so large, northern Taiwan was significantly affected. News reports indicated 37 people died, and typhoon damages were estimated to be over $10 million. Landslides on steep terrain swept away homes and even apartment complexes, while major flooding of homes and business occurred in the capital city of Taipei where about 225 mm of rain fell in about 36 h. Other rain gauge data indicated amounts between 150 and 250 mm across extreme northern Taiwan during a 4-day period from 16 to 20 August. In addition, a 600-m orographic peak in this area received nearly 750 mm.

Hours later, Typhoon Winnie made landfall in the eastern coastal province of Zhejiang, China, or about 260 km south of Shanghai. Approximately 30 million people were affected in the provinces of Zhejiang, Fujian, Jiangsu, and Shandong. Over 140 deaths and 3000 injuries were reported. This made Typhoon Winnie one of the deadliest and most destructive tropical cyclones to hit China in a decade. Over a million homes were damaged and economic losses totaled nearly $3 billion, primarily due to the flooding of farmland and crops. Rainfall totals exceeded 200 mm at several stations in

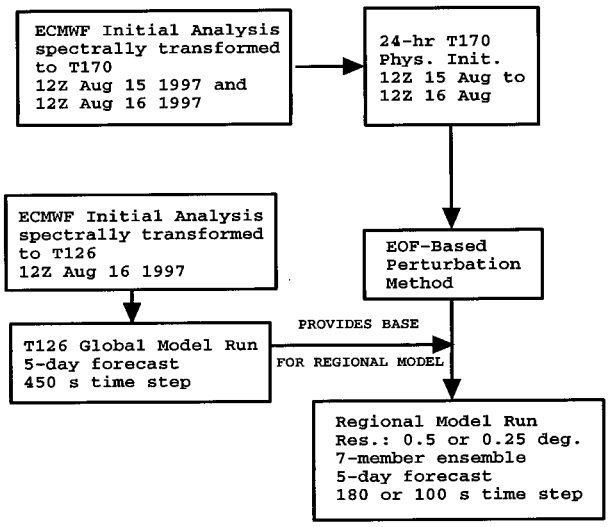

FIG. 2. Flowchart for Typhoon Winnie experiments.

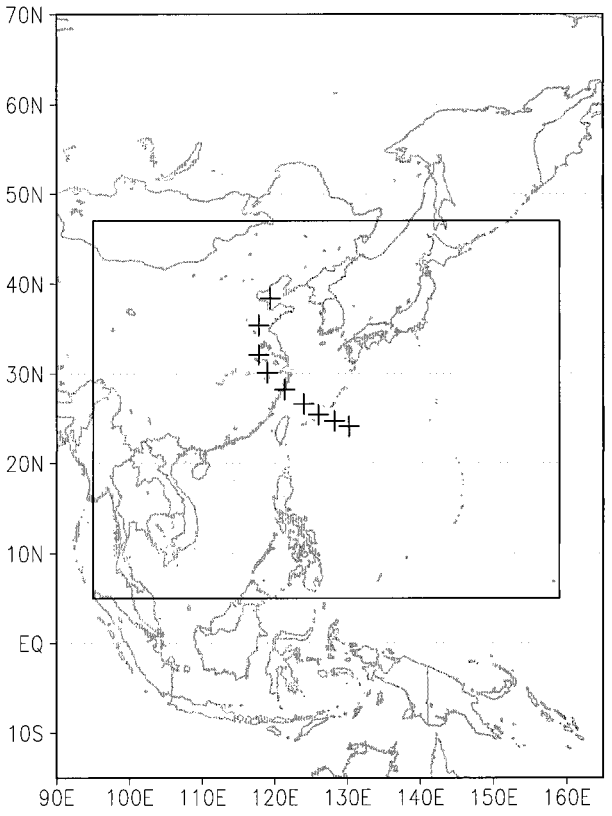

FIG. 3. Map showing the regional model domain size for the 0.5° lat experiment (solid line). The crosshairs indicate a portion of Typhoon Winnie's observed track.

eastern China as Winnie raked the northeastern China coast. At 0000 UTC 19 August, the last advisory was issued by the Joint Typhoon Warning Center as the cyclone was falling apart over the landmass of Manchuria. The remnant low pressure cell continued to recurve to the northeast (Dillon and Andrews 1997).

4. Ensemble forecast procedure

Two experiments, outlined in Fig. 2, were performed with the use of the FSUNRSM and the EOF-based perturbation method. All numerical experiments began at 1200 UTC 16 August 1997 while Typhoon Winnie was located nearly 1000 km to the east of Taiwan. At this time, maximum sustained surface winds were estimated near 41 m s^{-1}. To begin the procedure, European Centre for Medium-Range Weather Forecasts (ECMWF) global data at a resolution of T-106 were utilized. These data were then interpolated to a T-126 Gaussian transform grid for the global model integration. Furthermore, the ECMWF reanalysis data showed a well-defined and sufficiently deep tropical cyclone in the correct location, and thus a synthetic vortex was deemed unnecessary.

The main experiment began with a 24-h T-170 physical initialization procedure using the control analyses from day −1 and day 0. This powerful technique assimilates satellite-derived observed rainfall distributions along with calculated surface fluxes of moisture to produce a physically consistent and more realistic spinup of the initial state. The key to the spinup procedure is a Newtonian relaxation, where select variables are ''nudged'' toward prescribed values during a 24-h preintegration period. Upon integrating the FSUGSM, the rainfall patterns and surface moisture fluxes as well as the wind and mass fields appear more robust (Krishnamurti et al. 1991).

Then, the generation of perturbations was carried out via the EOF-based perturbation method whereby the first three eigenvectors were added (subtracted) to (from) the unperturbed, physically initialized analysis. Last, the regional model, which encompasses approximately 42° latitude (from 5° to 47°N) and 64° longitude (from 95° to 159°E), was integrated using a 0.5° latitude resolution. The regional domain for this experiment is illustrated in Fig. 3.

5. Results

a. EOF-based perturbations

After the randomly perturbed forecast is completed, EOF analysis begins on the two time series of wind and temperature differences (beginning with hour 6 and ending with hour 36). Figure 4 depicts the normalized principal component (PC) values for the wind time series at 1000 hPa. The first three principal components shown across the top of the figure are used in constructing the ensemble as these PCs show the largest growth rate and explain the most variance during the 36-h forecast. Within the first 12–15 h, the primary eigenmode exhibits the most rapid growth while the second and third modes do not grow as rapidly. Still, upon comparing modes two and three with the remaining six eigenmodes there

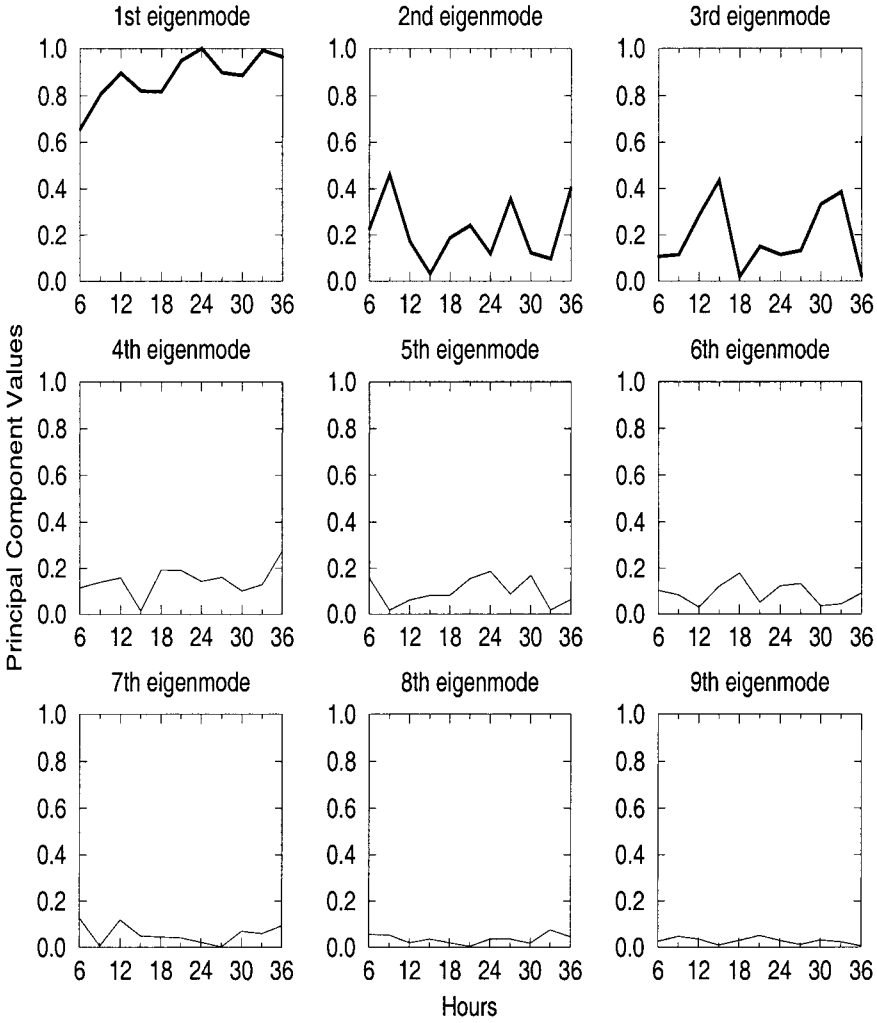

FIG. 4. Principal component values (amplitudes) of the wind field (1000 hPa) for the first (upper left) through the ninth (lower right) eigenmodes viewed from left to right.

is a noticeable difference as the last six modes oscillate quickly in time and remain near zero. It has also been shown that the largest initial amplitudes (hour 0) do not always correspond to the largest growth rate (Zhang 1997). The latter is the most important factor in determining which ensemble perturbations to use.

The next step is to add and subtract these fast growing eigenmodes to and from the initial unperturbed analysis, thereby reducing any model biases. It is plausible that the ensuing model integrations will adequately sample the forecast possibilities along these dynamically unstable modes and thus lead to an optimal ensemble spread. The first-order initial eigenvector (perturbation) fields for the 1000-hPa winds are displayed in the upper panel of Fig. 5. The lower panel depicts the error growth at hour 36. As a reference, Typhoon Winnie is located near 23.9°N, 130.5°E at hour 0 while at hour 36 it is centered near 26.8°N, 123.5°E. Clearly, the initial perturbation patterns are spatially correlated and well organized. Furthermore, the maximum initial amplitudes are associated with areas of robust weather disturbances, such as Typhoon Winnie. By hour 36, the perturbation maxima have doubled or even tripled in size near the typhoon. Rapid error growth has occurred. This can also be seen at other vertical levels and with other variables, such as temperature.

b. Typhoon Winnie track prediction

An ensemble forecast generates a tremendous amount of information, which must be clearly and concisely interpreted for a truly successful forecast. The value of an ensemble forecast can be decreased significantly by incorrectly or incompletely displaying the results. In this case, a single forecast will often prove more valuable. For hurricane prediction, usually the first items explored are the track forecasts. Using an ensemble technique, three different types of statistical track forecasts can be derived. The first, a simple ensemble mean, is the easiest to compute, but it gives equal weight to each member.

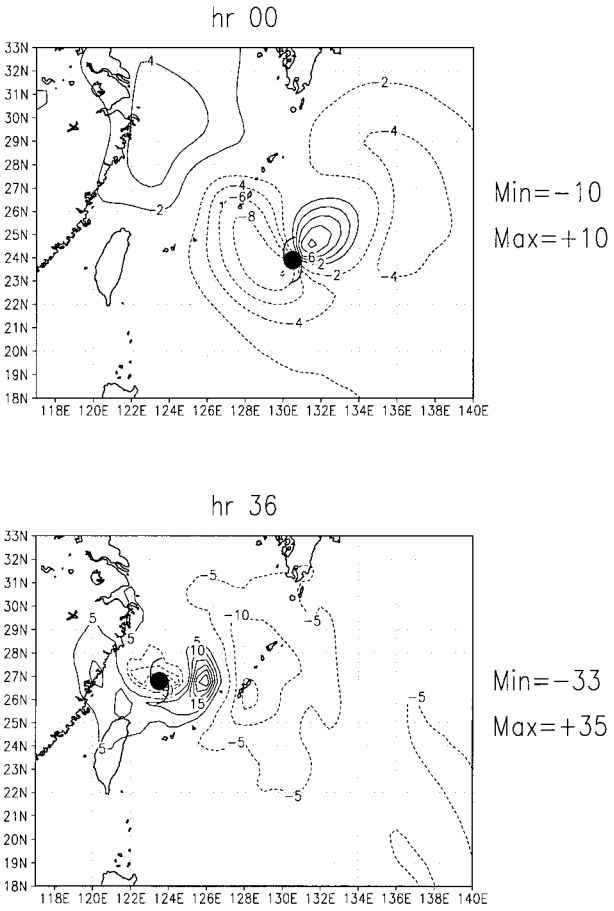

FIG. 5. The 1000-hPa primary eigenvector wind field (perturbations) (m s^{-1}) for hour (top) 00 and (bottom) 36.

Hence, an outlying track forecast is given an equal probability of occurring when compared to the others. A second method usually remedies this, however. It is often termed the cluster mean because it applies to ensemble members whose forecasts are grouped, or clustered, near each other. This method is only effective if there is an acceptable amount of divergence among the tracks. When that condition is met, then the most probable track forecast can be estimated by examining the cluster mean with the largest number of tracks. In addition, probabilities can be assigned to other cluster means. The final averaging method examines the model output at hour 12 and discards any gross outlying forecast compared to the observed. Then, a selected mean is performed over the remaining tracks. One must take great care, however, so that valuable information is not discarded too quickly.

Figure 6 shows the ensemble track forecasts for the 0.5° latitude regional simulation. Both the control and mean forecast perform well as position errors remain below 100 km through 60 h. The control forecast is initialized with the best guess observations, and, not unexpectedly, it often produces a superior forecast, especially during the first 48 h. The ensemble mean forecast, in theory, should also be highly skillful if the full spectrum of the error probability distribution is realized. For this case study, a classically recurving tropical cyclone is well entrenched in the synoptic flow. By examining the spread of the six perturbed members, two distinct track clusters are apparent, one to the north and east of the observed track and one to the south and west. Hence, it appears that some, and possibly a majority, of the total forecast variance is accounted for, suggesting that no further members are necessary to determine the mean as the most dynamically unstable modes have apparently been sampled. Further work is needed to see the impact of additional, more stable perturbations. Ideally, a majority of the track forecasts would be clustered closer to the mean. Furthermore, after day 3, the ensemble and control position errors increase rather rapidly as the weak low pressure system that once was Typhoon Winnie recurved over the landmass of eastern China. The time evolution of the position variance, however, remains stable between 150 and 200 km indicating a fairly reliable forecast. During the 5-day forecast, both the ensemble mean and unperturbed control track provide the best guidance for this particular case study. This provides a high degree of confidence for a forecaster or end user. On average, this ensemble prediction system will provide a higher degree of forecast skill, but it may not always do so for each instance (Zhang 1997).

c. Typhoon Winnie intensity prediction

The intensity issue is a major component of tropical cyclone prediction, and it is well known that intensity forecasts, in general, have less skill than the position forecasts. It is likely, however, that ensemble techniques can increase the skill by providing a range of possible forecasts in addition to the ensemble mean. Other output, such as probability distribution charts and station time series, can add insightful information to the forecast.

1) WIND FIELD FORECAST

Figure 7 depicts a time series of Winnie's maximum surface layer wind speed in meters per second. The vertical bar at hour 48 indicates when Winnie made landfall in east China. The observed intensities are estimated at the JTWC from the satellite-based Dvorak technique, which does have various limitations, especially for a cyclone with such an unusual eye structure. Using this technique on typhoons in the northwest Pacific Ocean basin yields an average central pressure error of 10 mb with a standard deviation of 9 mb (Martin and Gray 1993). As Typhoon Winnie made landfall, the maximum sustained winds were estimated to be 39 m s^{-1}. The closest Dvorak current intensity number is 4.5, or 40 m s^{-1}. On average, however, these intensity numbers are better

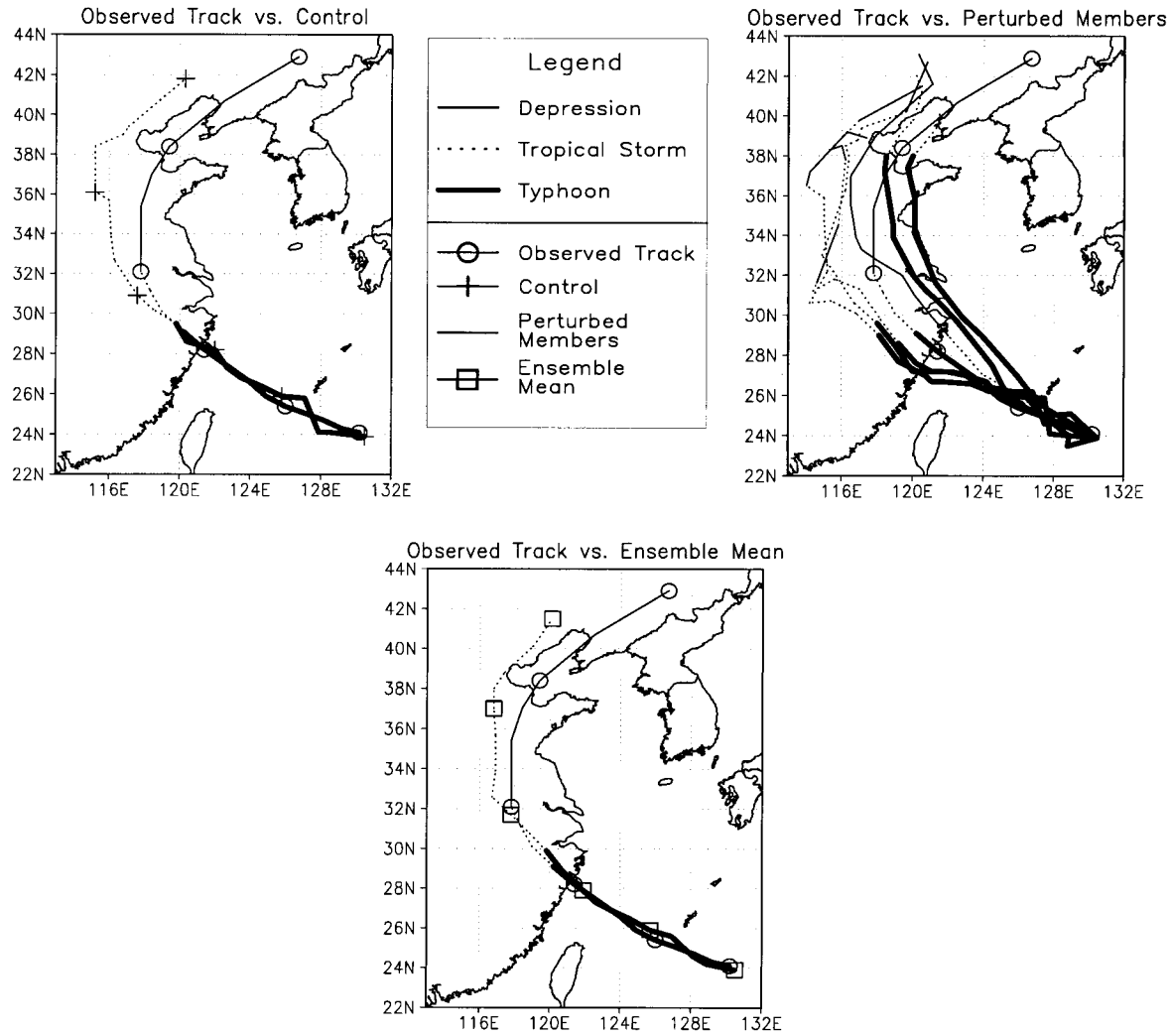

FIG. 6. Typhoon Winnie track forecasts from the 0.5° lat experiment.

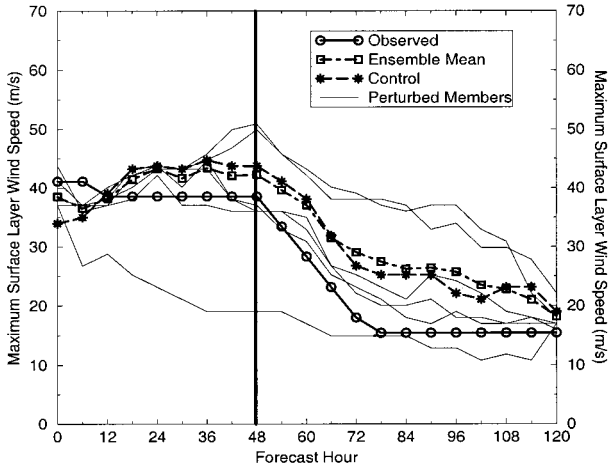

FIG. 7. Typhoon Winnie intensity time series for the 0.5° lat experiment. The vertical bar denotes the time of observed landfall.

suited for a range of possible maximum wind speeds. In this case, the range would be from 31 to 46 m s^{-1}. At the time of landfall, two members are clearly stronger, three others are close to the observed, and one is significantly weaker. This outlier has been omitted from the ensemble mean through the remainder of this study because it sufficiently diverges from the other members within the first 12 h. Since the model integrations take slightly more than 12 h to complete, a decision to omit this outlying member can be made at that time. It is best to exercise caution, however, so that valuable forecast information is not discarded too quickly. For this case study, both the control and mean forecasts perform well with the ensemble mean slightly better through hour 66. Once again, as the control and mean forecasts remain quite close to each other, this should give a forecaster additional confidence in the landfall intensity of Typhoon Winnie (approximately 40 m s^{-1}). Later, as the storm weakens over land and enters the midlatitudes, the ensembles show a bias toward stronger intensities.

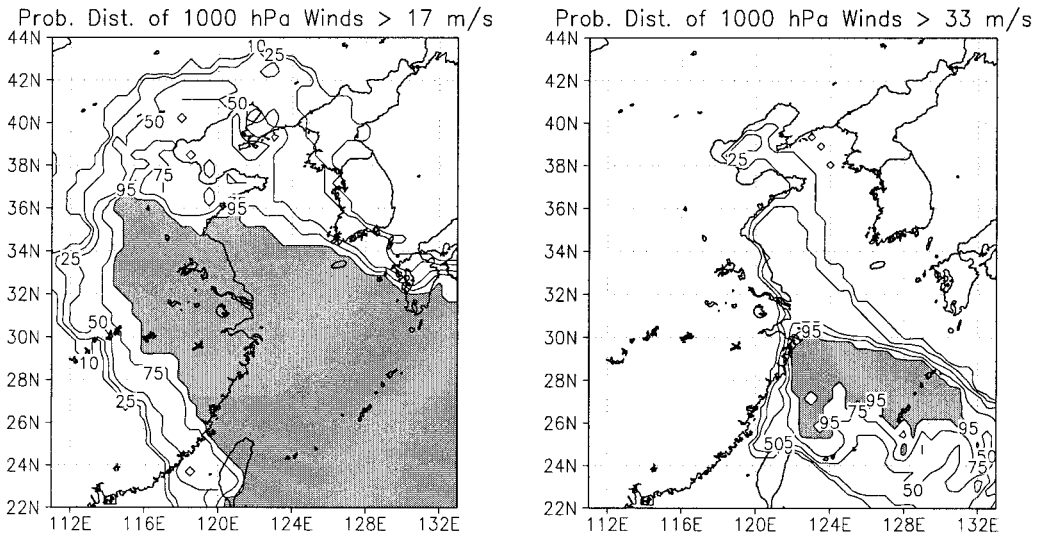

FIG. 8. Probability distribution of wind speeds greater than (left) 17 and (right) 33 m s^{-1}. Values greater than 95% are shaded.

Perhaps a more beneficial product from an ensemble intensity forecast is a probability distribution map. These types of charts are constructed assuming that each ensemble member is equally plausible. At each model grid point, the probability, P, of any variable, X, falling within a specified range, $x_L < X < x_U$, is equal to the number of member forecasts within that range, N_{sample}, divided by the total number of ensemble members, N_{total}. This can be expressed as

$$P_X\{x_L < X < x_U\} = \frac{N_{\text{sample}}}{N_{\text{total}}}. \quad (1)$$

Obviously, this type of map is most useful for a large number of ensemble members (about 30 or more). In this case, only six members are represented. Figure 8 shows the probability distribution of 1000-hPa wind speeds greater than 17 m s^{-1} (left) and 33 m s^{-1} (right). Values greater than 95% are shaded. From these charts, a large area is likely to experience tropical storm force winds, including the northern half of Taiwan and a good portion of eastern China, including Shanghai. Half of the ensemble members predict winds above 33 m s^{-1} only over extreme northern Taiwan and a small region of the Chinese coastline between 28° and 31°N. One-quarter of the members bring these winds along the coast up to 35°N. Hence, forecasters may be able to give advance warning of tropical storm or hurricane force winds based upon these types of probability maps. For winds greater than a particular threshold, one could assign high confidence of occurrence to all areas above the 95% level.

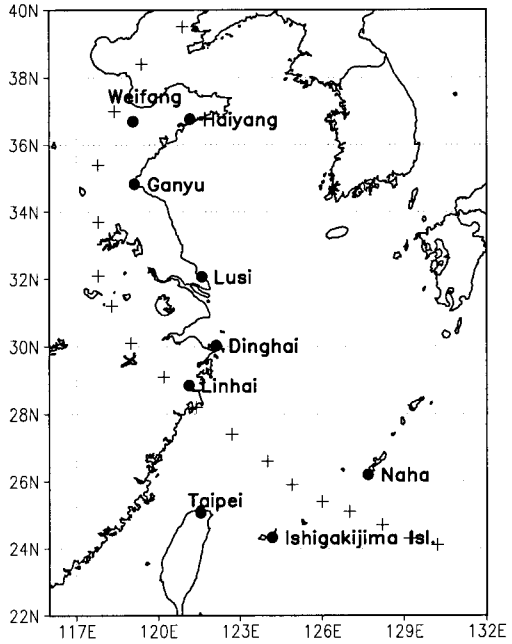

FIG. 9. Reference map showing nine stations and the track of Typhoon Winnie (crosshairs).

2) MEAN SEA LEVEL PRESSURE FORECAST

One additional intensity predictor—mean sea level pressure—is now examined. Unlike model-derived wind speeds, this variable is easier to compare with ground station observations. As a reference, the map in Fig. 9 displays the track of Typhoon Winnie (crosshairs) along with nine stations to be examined through the remainder of this study. These stations can be further divided into three geographical groups of three. In Fig. 10 one representative from each of the three groups is chosen, and a mean sea level pressure time series is then generated for Naha (upper panel), Dinghai (middle panel), and

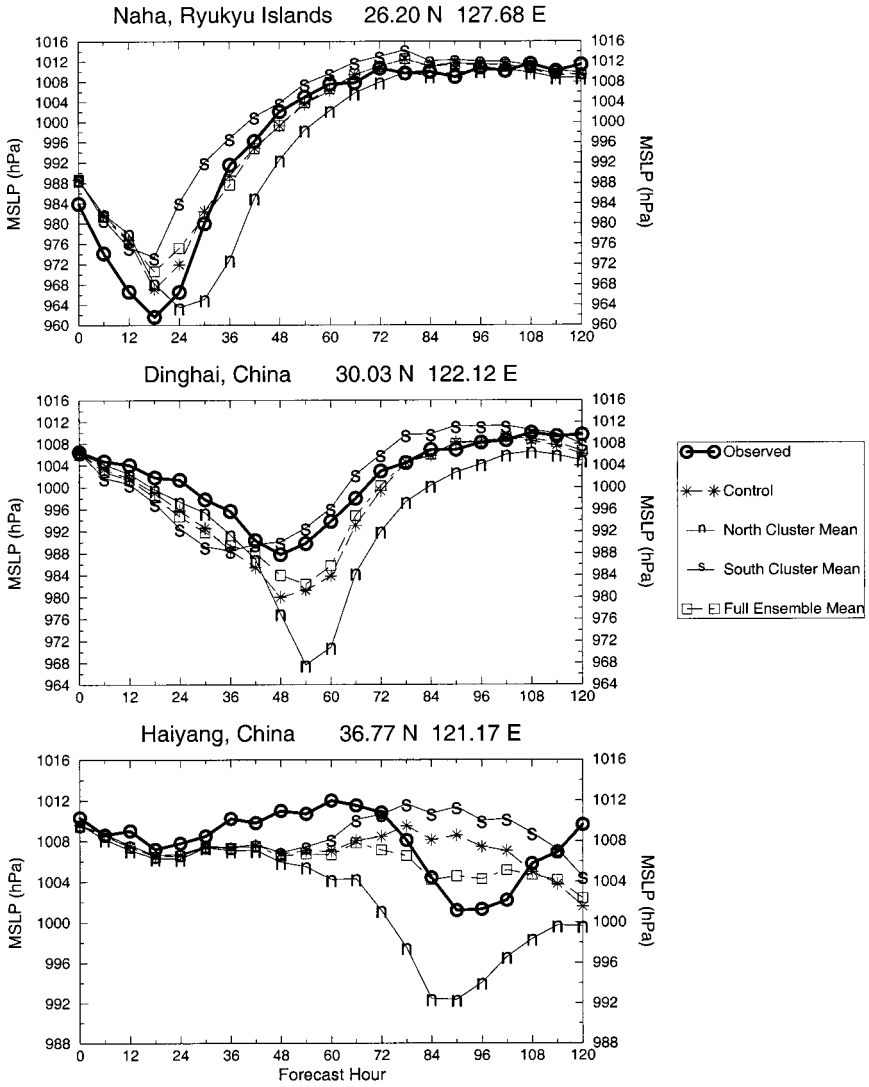

FIG. 10. Time series of mean sea level pressure (hPa) for (top) Naha, (middle) Dinghai, and (bottom) Haiyang. The thick solid line with circles denotes the observed; the thin dashed line with stars denotes the control forecast; the thin solid lines marked n and s denote the north and south cluster means, respectively; and the thin dashed line with squares denotes the full ensemble mean.

Haiyang (lower panel). The observed, control, north and south cluster means, and full ensemble mean are plotted for each station. The north and south cluster means contain just two and three members, respectively, but it is felt that these means adequately describe the range of the forecasts.

At Naha, the model-derived initial pressure is approximately 4 hPa higher than the observed, and through the first 24 h of the forecast, this predicted sea level pressure positive bias continues. This type of error is specific to the model and the tropical cyclone, but an end user should take note of any bias when successive model runs are made on a particular storm. In addition, after hour 24, the north and south cluster means do surround the ground truth and provide an ''envelope'' of possible outcomes. Indeed, within this envelope the ensemble mean and control perform quite well. For Dinghai, even though all model pressures are slightly lower than the observed during the first 42 h, the ensemble mean narrowly outperforms the control forecast. The modeled typhoon in the north cluster, however, moves directly over the station resulting in a significant error along with a slight lag at hour 54. For Haiyang, the focus is on the final 2 days of the forecast when the weakened typhoon passes by the station. This is a great example of why an ensemble can be useful. Despite a large spread among member forecasts, the ensemble mean greatly reduces the intensity error, even at day 4 of the forecast.

d. Typhoon Winnie precipitation prediction

Along Typhoon Winnie's destructive path, heavy rains saturated portions of northern Taiwan and eastern China, leading to, among other effects, landslides and flooded crops. Heavy precipitation events like this one often occur with landfalling tropical cyclones, and in order to save lives and safeguard property, it is important to foretell such events in advance. Precipitation forecast skill, however, is usually below that of all other model variables. Inaccurate convective parameterizations, coarse model resolutions, and the inherent mesoscale variability of rainfall may all lead to poor forecasts. By performing a high-resolution integration (0.5° latitude) and using different ensemble output techniques, it is hoped that a successful prediction of the typhoon flood event can be realized. The precipitation data from the model integrations will be compared with both satellite and rain gauge estimates.

First, the results from the 0.5° latitude resolution model simulation are displayed. Figure 11 shows postage stamp maps of day 1 accumulated precipitation. The ensemble mean is displayed in the upper-left panel, the control in the upper right, while the remainder of the members are shown below. Within the first 24 h, heavy precipitation encircles the typhoon center as three members produce over 200 mm of rain. In addition, a relative precipitation minimum of less than 100 mm is evident near the typhoon center. This gap covers an area greater than 10 000 km^2 and is indicative of a large eye feature. In Zhang's (1997) 1° latitude model simulations, there was no evidence of a minimum in precipitation at the cyclone center. However, by using a higher-resolution model (0.5° latitude) and including physical initialization (which assimilates the initial observed rainfall distribution), this case results is a much better defined typhoon.

Moreover, from the forecast track output (not shown), three ensemble members—EOF + 2, EOF + 3, and EOF − 1—are faster than the others through the first 48 h. This is also reflected in the day 1 precipitation patterns, in which there is a noticeable spreading of the rainfall for the fast-moving cyclones. For these members, rainfall has already begun along the Chinese coastline by the end of day 1. A forecaster or end user must recognize that half of the perturbed members favor this faster and more southern scenario. This would put Taiwan and portions of eastern China in greater danger, and it would give them less time to prepare for a possible impact.

By examining the 5-day precipitation fields from the six perturbed forecasts (Fig. 12), it is clear that there are two preferred swaths of precipitation, one associated with a northern cluster of ensemble members (EOF + 1 and EOF − 2) and another with a southern cluster (EOF + 2, EOF − 1, and EOF − 2). Over the ocean east of Taiwan, the north cluster exhibits a northwest–southeast-oriented swath of heavy precipitation. Amounts in some locations are forecast to exceed 300 mm. Over land areas, however, the rainfall totals are much less. The ensemble members that make landfall much farther south, on the other hand, do produce significant precipitation across portions of northern Taiwan and eastern China. In this case, a northeast–southwest-oriented band is aligned along the Chinese coast from 24° to 30°N. West of 123°E, a bimodal rainfall distribution results. Where one cluster predicts meager amounts of precipitation, the other forecasts an abundant amount and vice versa. Once again, forecasters should be mindful of these two distinct possibilities, and that the most likely outcome (the ensemble mean) will be a compromise between these two modes.

In order to benefit further from the ensemble forecast, Fig. 13 displays the probability distribution of precipitation greater than 50 (upper left), 100 (upper right), 150 (lower left), and 200 mm (lower right). Values above 75% are shaded. This type of map will be particularly useful to forecasters as they can pass probability information on to emergency management and the general public. As expected, the shaded area decreases as the probability threshold increases. A good portion of Taiwan and eastern China is likely to receive over 50 mm of precipitation during the 5-day forecast time period. In addition, the extreme northern tip of Taiwan has about an even chance of total rainfall greater than 150 mm, while the threat is relatively high for coastal eastern China between 28° and 30°N. The chances of most land areas experiencing rain amounts greater than 200 mm, however, are much slimmer. These results compare favorably with the observed rainfall distributions over northern Taiwan and eastern China (as seen in the lower-left panel of Fig. 14). In other words, where there is a high probability of occurrence (shaded area), the observations generally support this.

Figure 14 shows 5-day precipitation totals from the control (upper left), regular ensemble mean (upper right), and observed (bottom). The observed rainfall data consist of both satellite estimates and rain gauge measurements from 22 Taiwanese stations and 83 eastern Chinese stations. Satellite rainfall estimates are generally more accurate over the ocean when compared to land areas. This is because the rainfall retrieval algorithm uses rain rates gathered mainly over oceanic areas, and only the 85-GHz brightness temperatures were used for land areas (Tibbetts 1999). Thus, these data must be used with caution. For example, along the Chinese coastline, the station data may not blend perfectly with the satellite-derived quantities. The control and ensemble mean forecasts possess similarities, and, in general, each is a good approximation to the observed, except over the higher terrain of Shandong Province north of the Yellow Sea. Here, precipitation is underforecast. This shows that future work is needed in numerical modeling of precipitation for forecast days 4 and 5. The control produces the most precipitation while showing more detail (e.g., the narrow bands of heavy rain over

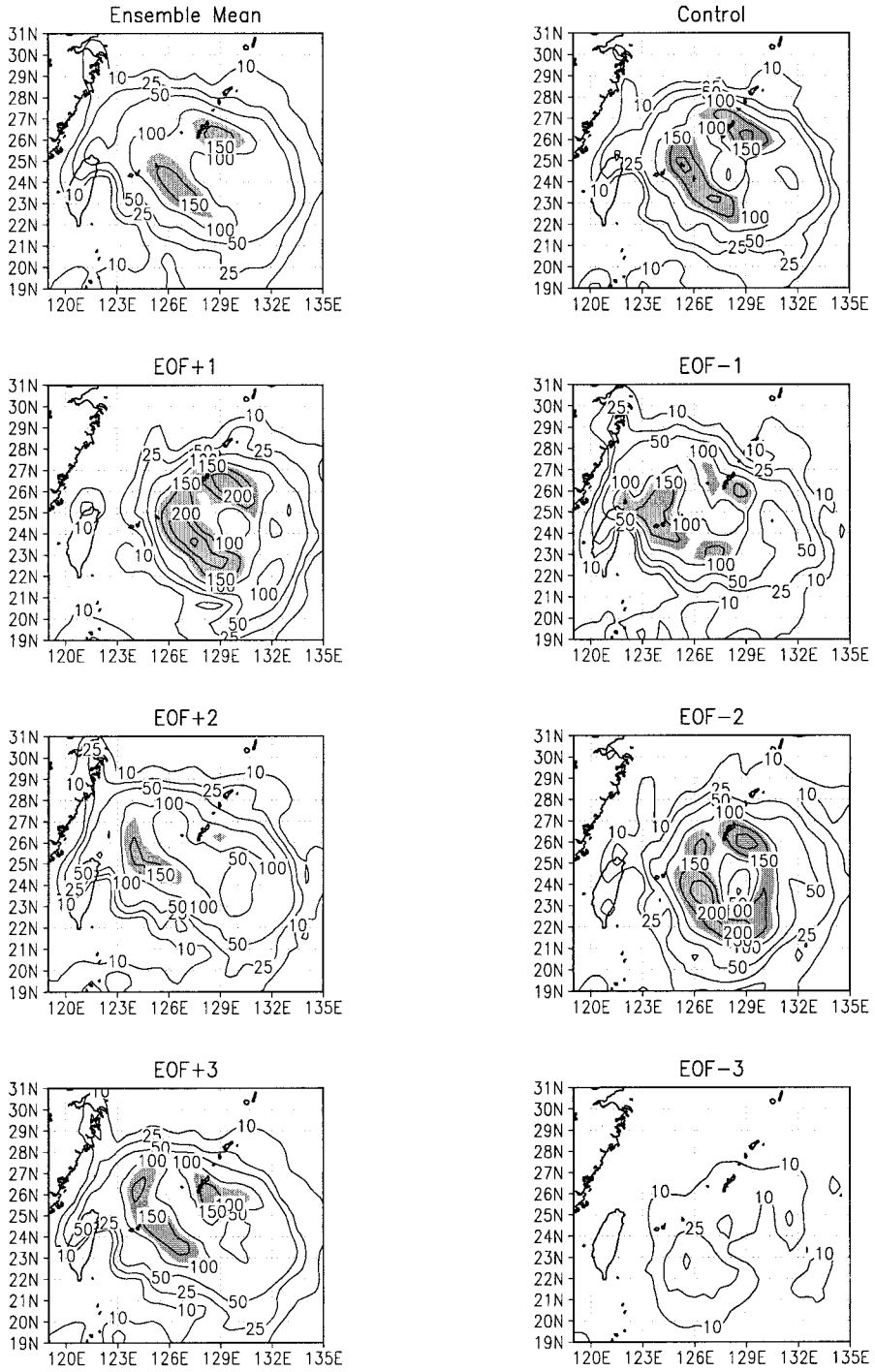

FIG. 11. Day 1 accumulated precipitation (mm) postage stamp maps for each ensemble member and ensemble mean for the 0.5° lat simulation. Amounts greater than 125 mm are shaded.

the ocean). The area near northern Taiwan is well predicted, but in the control too much rain falls over inland areas of eastern China. Thus, upon correlating the control to the observed, the coefficient is 0.56. Some of the problems are remedied, however, by the mean forecast (correlation of 0.65), which gives a much smoother representation while still retaining areas of heavy precipitation that are common to most members.

Next, time series and related statistics of accumulated rainfall from the aforementioned nine stations are compiled. Table 1 summarizes the results. These nine stations were chosen due to the high precipitation amounts

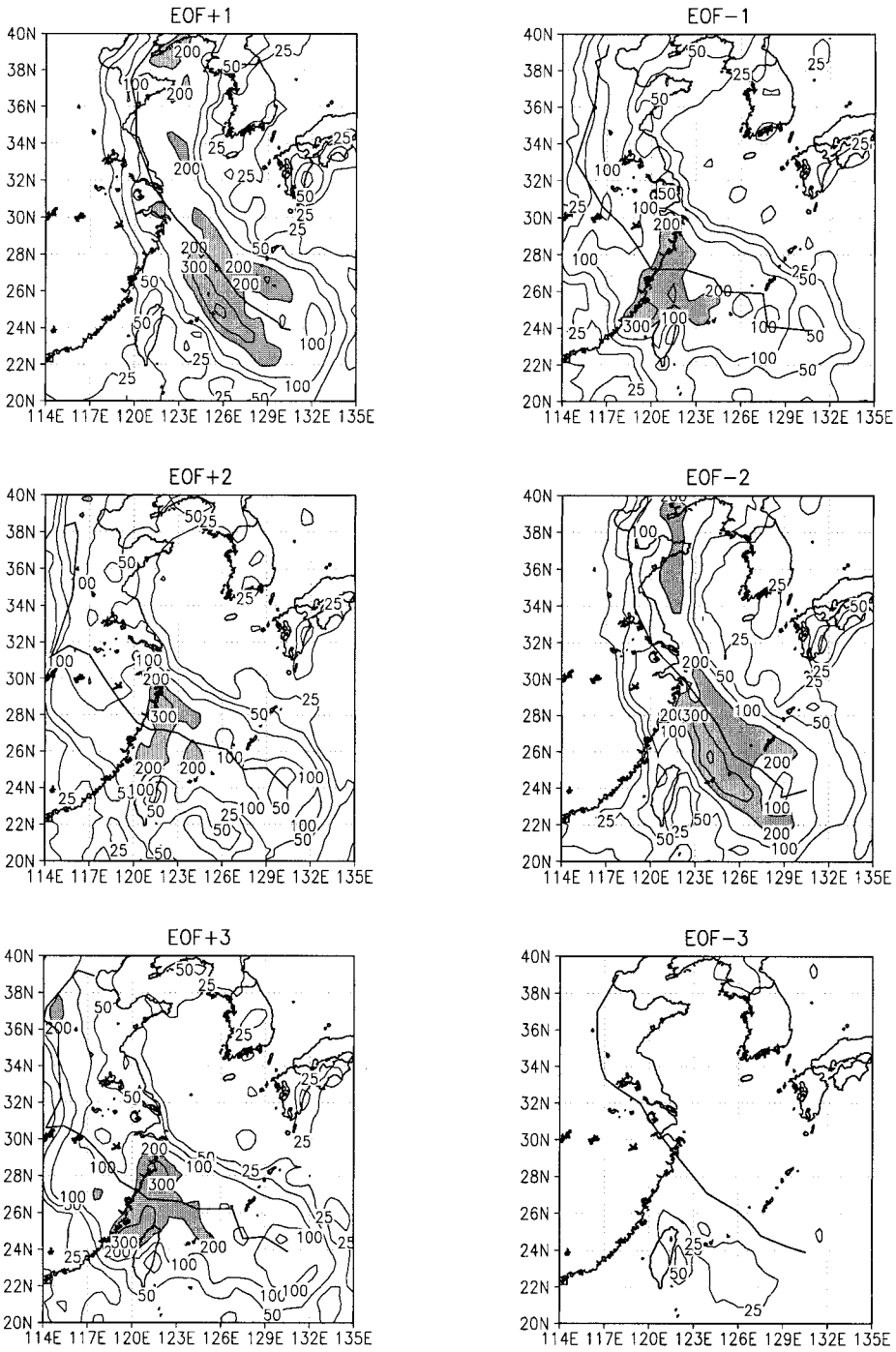

FIG. 12. The 5-day accumulated precipitation (mm) postage stamp maps for each perturbed ensemble member from the 0.5° lat simulation. Amounts greater than 200 mm are shaded. The solid line drawn on each map indicates the simulated track for that ensemble member.

that they received. In all cases except one, the forecast spread (the ensemble mean plus or minus the standard deviation) is not sufficient to cover the final observed rainfall amount. It is obvious, therefore, that for these stations, the model simply underforecasts the precipitation amounts, especially in the medium time range of days 4 and 5. Nevertheless, valuable information can be gained by examining these time series. At three of the stations, the maximum rain from any ensemble member exceeds the observed, while at least one forecast is quite similar to the observed at five locations. Accompanying this forecast is some probability of oc-

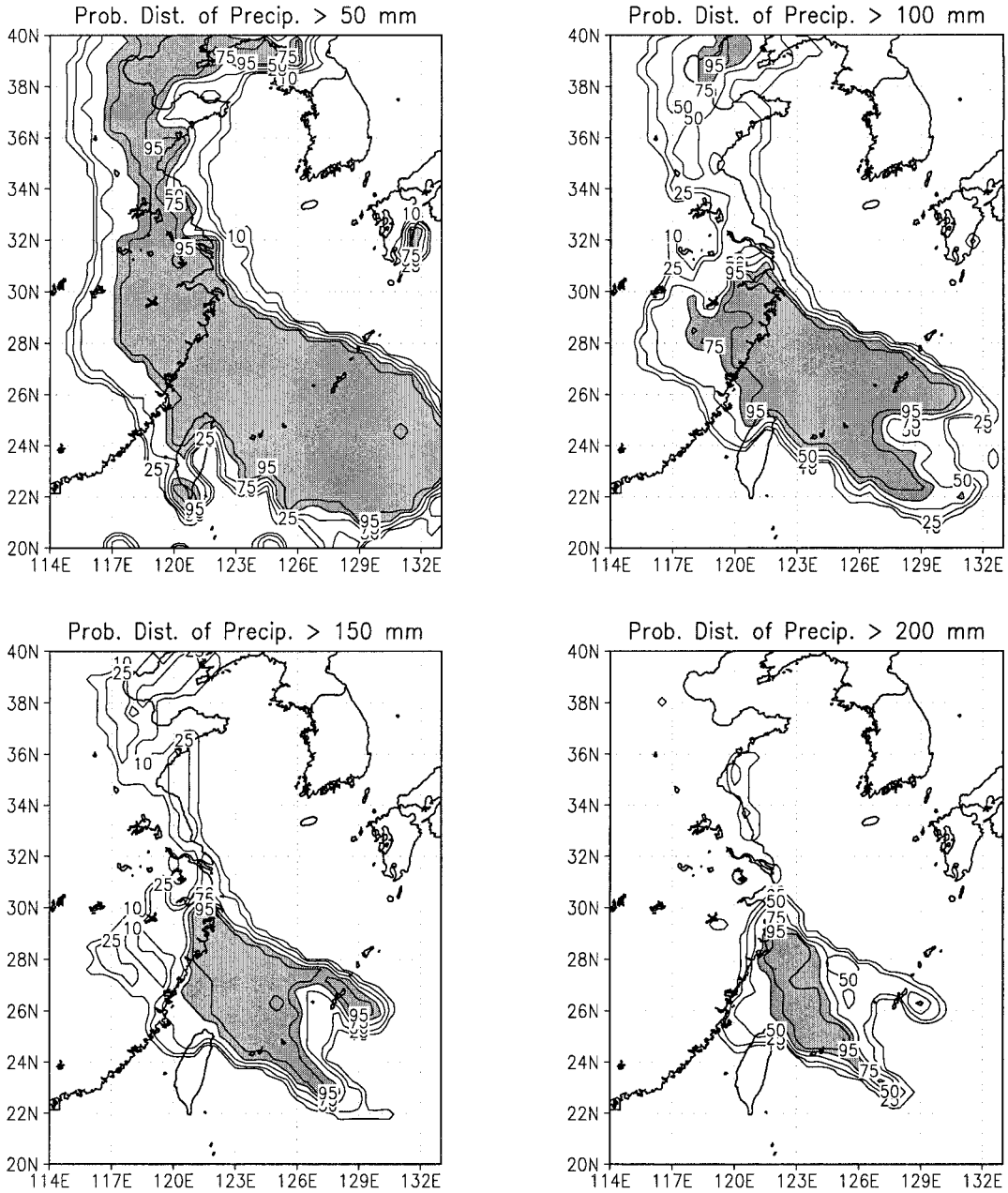

FIG. 13. Probability distribution of 5-day total precipitation for amounts greater than (upper left) 50 (upper right) 100, (lower left) 150, and (lower right) 200. Values greater than 75% are shaded.

currence, which, no matter how small, should not be disregarded. Because of the many uncertainties in rainfall prediction, forecasters should focus on possible outcomes and not just on the most statistically likely forecast. For the central group of stations affected by Winnie's core, the observed, control, north and south cluster means, and full ensemble mean is graphed in Fig. 15. The average error for the ensemble mean forecast is 39%.

The point precipitation (station) forecasts shown above are usually the most difficult to predict due to the large variability of rainfall. While almost all forecasts underestimate total precipitation at those nine stations, certainly at other stations rainfall amounts are overdone while at still others the forecasts are very close to the observed. Higher skill likely will be realized by objectively transforming these point values to a spatially averaged precipitation map, which shows the volume of total water over an area for a specified time interval. The higher skill achieved with this method is the current state of the art (Sigrest and Krzysztofowicz 1998).

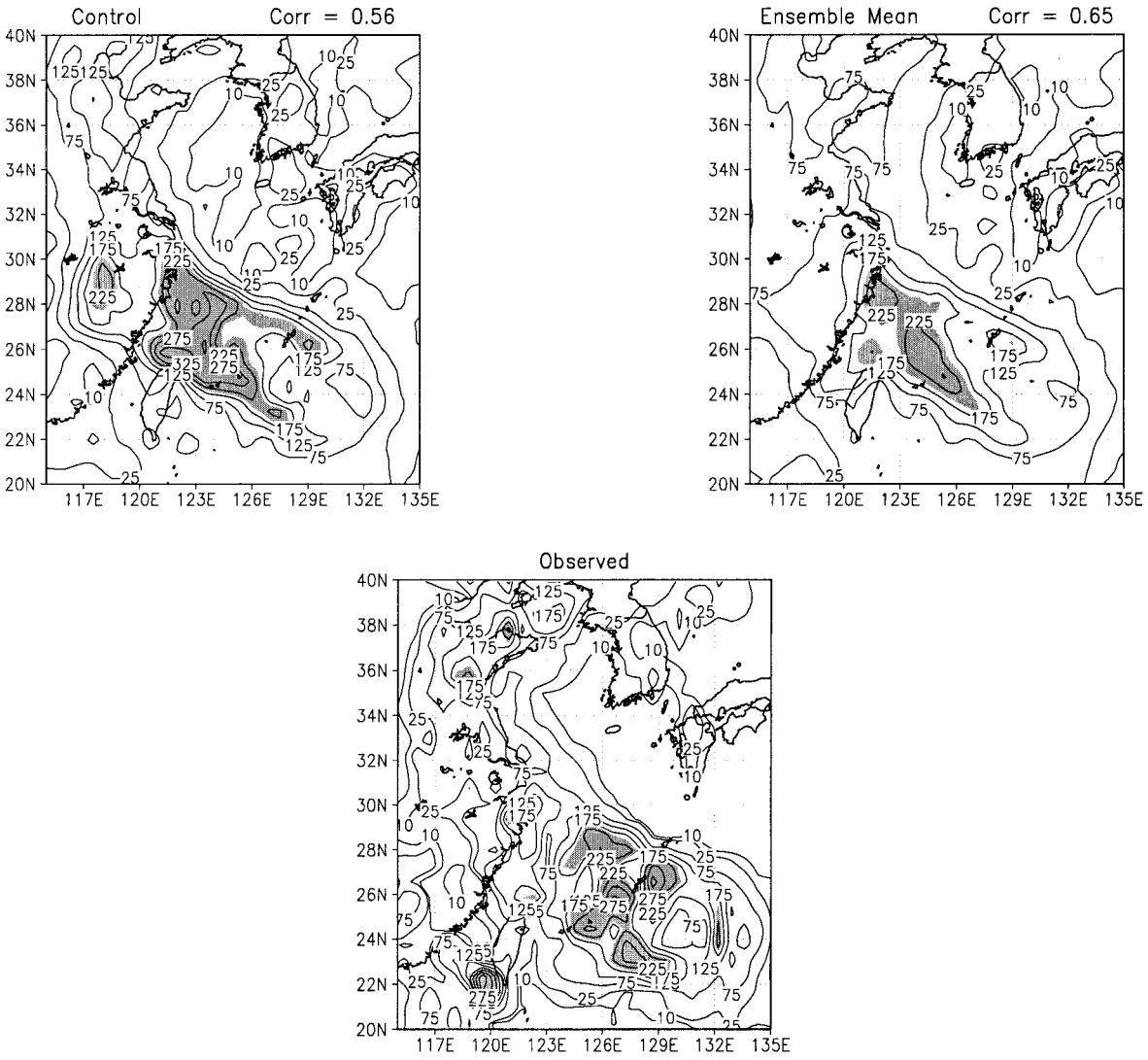

FIG. 14. The 5-day total precipitation (mm) from the 0.5° lat simulation for the (upper left) control, (upper right) ensemble mean, and (bottom) observed. Amounts greater than 200 mm are shaded.

Another set of forecasts are integrated using the same initial perturbations but with a higher-resolution regional mesh of 0.25° latitude. Briefly, the track forecasts show a similar degree of skill, but with a much larger spread (not shown). With a higher-resolution model, it is plausible that more chaotic effects and initial uncertainties are introduced, thereby increasing the likelihood of track divergence. In addition, the higher-resolution

TABLE 1. The 5-day station precipitation totals (mm) for the 0.5° lat model simulation.

Station	Lat–Long (°N–°E)	Closest Point grid (km)	Precipitation (mm)				
			Obs	Cntrl	Ensemble mean	Std dev	Max value
Naha	26.2–127.7	21.24	214.0	133.3	158.5	56.2	217.6
Ishigakijima	24.3–124.2	28.29	303.0	203.7	147.8	74.8	205.5
Taipei	25.1–121.6	9.48	234.9	157.7	157.8	39.8	249.7
Linhai	28.9–121.1	14.38	261.4	189.0	192.5	33.4	296.4
Dinghai	30.0–122.1	23.68	237.9	186.8	139.0	20.5	204.1
Lusi	32.1–121.6	15.82	160.7	66.2	81.3	70.9	144.5
Ganyu	34.8–119.1	22.27	214.4	132.2	73.8	79.6	132.2
Haiyang	36.8–121.2	15.52	278.6	40.6	86.5	63.6	180.9
Weifang	36.7–119.1	8.35	162.1	89.5	65.3	38.5	89.5

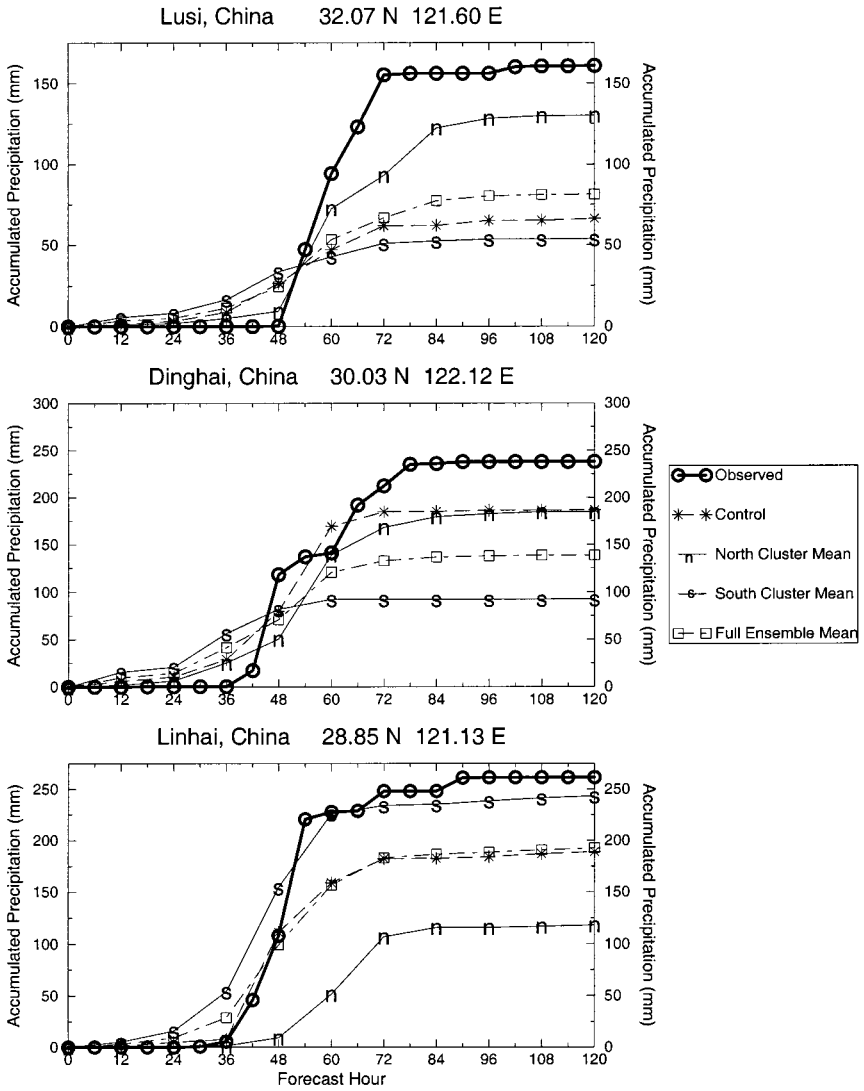

FIG. 15. Time series of 5-day accumulated precipitation (mm) from the 0.5° lat simulation for (top) Lusi, (middle) Dinghai, and (bottom) Linhai. The thick solid line with circles denotes the observed; the thin dashed line with stars denotes the control forecast; the thin solid lines marked n and s denote the north and south cluster means, respectively; and the thin dashed line with squares denotes the full ensemble mean.

forecast does not contain the ''intensity'' outlier observed in the 0.5° latitude case. The precipitation forecasts (not shown) give even more detail; the control forecast is even more skillful (correlation coefficient of 0.63). Also, the ensemble mean rainfall performs remarkably well during the first 2 days of the forecast. Thereafter, it suffers due to the strong bimodal distribution of the member forecasts. Thus, precipitation errors are similar to the 0.5° latitude simulation.

Furthermore, due to the bimodal 5-day rainfall distributions and the subsequent smoothing of the ensemble mean precipitation, the need arises for some type of compositing technique. One such method is applied to this case study with limited success. By comparing the track coordinates of each member to the ensemble mean track, the precipitation data from each member then can be transformed so that it falls along the mean track. A new mean rainfall pattern emerges. Obviously, there can be complications in this design, but for this case of a smoothly recurving typhoon, no serious obstacles were anticipated. This new mean improves the precipitation amounts at several of the stations in Table 1, but overall, the correlations are not any better than the ordinary ensemble mean. This new mean even slightly degrades the forecast in some areas.

6. Summary and conclusions

Through the use of a high-resolution regional spectral model with physical initialization and an EOF-based

perturbation technique, this study aims to assess the effectiveness of an ensemble forecast of Typhoon Winnie's track, intensity, and flooding rains. In this case, heavy rains over China and northern Taiwan were likely a consequence of 1) the core and spiral bands of Winnie, 2) frictional convergence along the Chinese coast, and 3) high topography.

In a high-resolution experiment, the track and intensity of Typhoon Winnie are well-predicted by both the ensemble mean and control (unperturbed) forecast. Given that the mean and control remain very close throughout the 5-day forecast period, an end user should gain additional confidence in the track and intensity prediction. Since the control is derived from the best guess initial conditions, one might expect this member to be among the best. Indeed, the control forecast is often given extra weight in an ensemble prediction. The ensemble mean track, however, should be superior only if the forecast uncertainty is properly sampled. Using an ensemble with a finite number of members, it is practically impossible to sample each and every direction. Nevertheless, by projecting empirical modes onto fast-growing directions in the model phase space, the EOF method gives an optimal range of possible forecast atmospheric conditions. The degree of success of this study and of the EOF method is not guaranteed, however, for every case. Many more simulations need to be performed involving a variety of different synoptic situations.

In addition to the track and intensity charts, an assortment of useful products can be created from an ensemble forecast. Among these are postage stamp maps, cluster mean charts, probability distribution maps, and station time series. The focus of this study is on the precipitation products from the ensemble members. As mentioned, precipitation is a very difficult variable to forecast even when other variables are well predicted. For the 0.5° latitude simulation, the control forecast produces realistic precipitation patterns, including mesoscale bands of enhanced precipitation. The ensemble mean is a little smoother, but heavy rainfall amounts greater than 200 mm still show up near the Chinese coast. By examining nine stations that received heavy precipitation, however, most of the forecasts did not produce sufficient precipitation. The best skill occurred near and to the north of where Typhoon Winnie made landfall.

Numerical weather prediction of rainfall, especially rare event flooding cases, is very challenging, even when a storm's track and intensity are correctly modeled. A discontinuous, derived quantity like precipitation often possesses much variability in space and time. Thus, it is best to examine each individual ensemble member carefully in order to determine the maximum amount possible at any one location. In addition, with the implementation of a type of precipitation compositing, improved rainfall amounts for typhoon flood cases may aid forecasters in the future. This technique shows some promise, provided that the tropical cyclones do not propagate erratically or traverse over mountainous regions.

Acknowledgments. This work was supported by NSF Grant ATM-9710336, NASA Grant NAG8-1199, NASA Grant NAG5-4729, NOAA Grant NA77WA0571, and NOAA Grant NA86GP0031.

APPENDIX A

FSU Global Spectral Model

An outline of the FSU Global Spectral Model:

- Independent variables: (x, y, σ, t)
- Dependent variables: vorticity, divergence, surface pressure, vertical velocity, temperature, and humidity
- Horizontal resolution: triangular truncation
- Vertical resolution: 14 layers between roughly 10 and 1000 mb
- Semi-implicit time differencing scheme (Robert et al. 1972)
- Envelope orography (Wallace et al. 1983)
- Centered differences in the vertical for all variables except humidity, which is handled by an upstream differencing scheme
- Fourth-order horizontal diffusion (Kanamitsu et al. 1983)
- Kuo-type cumulus parameterization (Krishnamurti and Bedi 1988)
- Shallow convection (Tiedtke et al. 1988)
- Dry convective adjustment (Kanamitsu 1975)
- Large-scale condensation (Kanamitsu 1975)
- Surface fluxes via similarity theory (Businger et al. 1971)
- Vertical distribution of fluxes utilizing diffusive formulation where the exchange coefficients are functions of the Richardson number (Louis 1979)
- Long- and shortwave radiative fluxes based on a band model (Harshvardan and Corsetti 1984; Lacis and Hansen 1974)
- Diurnal cycle (day–night by variation of zenith angle)
- Parameterization of low, middle, and high clouds based on threshold relative humidity for radiative transfer calculations (Slingo 1985)
- Surface energy balance coupled to the similarity theory (Krishnamurti et al. 1991)
- Nonlinear normal mode initialization: five vertical modes (Kitade 1983)
- Physical initialization (Krishnamurti et al. 1991)

APPENDIX B

FSU Regional Spectral Model

An outline of the FSU Regional Spectral Model (Cocke 1998):

- One-way, nested perturbation model

- Compatible with the FSUGSM; dynamics, physics, and vertical structure are the same
- Mercator projection in the horizontal
- Regional fields are composed of a base field (via the FSUGSM) plus a high-resolution perturbation field
- Perturbations are relaxed to zero at the lateral boundaries
- Orography derived from the perturbation geopotential height at the surface
- Elliptic truncation (analogous to triangular truncation)

REFERENCES

Buizza, R., and T. N. Palmer, 1995: The singular-vector structure of the atmospheric global circulation. *J. Atmos. Sci.,* **52,** 1434–1456.

Businger, J. A., J. C. Wyngaard, Y. Izumi, and E. F. Bradley, 1971: Flux profile relationship in the atmospheric surface layer. *J. Atmos. Sci.,* **28,** 181–189.

Chen, L., 1995: Tropical cyclone heavy rainfall and damaging winds. *Global Perspectives on Tropical Cyclones,* R. L. Elsberry, Ed., WMO/TD 693, World Meteorological Organization, 261–289.

Cocke, S., 1998: Case study of Erin using the FSU Nested Regional Spectral Model. *Mon. Wea. Rev.,* **126,** 1337–1346.

De, U. S., and K. S. Joshi, 1998: Natural disasters and their impacts on developing countries. *WMO Bull.,* **47,** 336–343.

Dillon, C. P., and M. J. Andrews, cited 1997: Western North Pacific tropical cyclones: 14W STY Winnie. 1997 Annual Tropical Cyclone Rep., U.S. Naval Pacific Meteorology and Oceanography Center West/Joint Typhoon Warning Center, Naval Base Pearl Harbor, HI. [Available online at http://www.npmoc.navy.mil/products/jtwc/1997_atcr/ch3/14ww.htm.]

Hamill, T. M., and S. J. Colucci, 1998: Evaluation of Eta–RSM ensemble probabilistic precipitation forecasts. *Mon. Wea. Rev.,* **126,** 711–724.

Harshvardan, and T. G. Corsetti, 1984: Longwave parameterization for the UCLA/GLAS GCM. NASA Tech. Memo. 86072, Goddard Space Flight Center, Greenbelt, MD, 52 pp.

Kanamitsu, M., 1975: On numerical prediction over a global tropical belt. Dept. of Meteorology Rep. 75-1, The Florida State University, Tallahassee, FL, 282 pp.

——, K. Tada, K. Kuda, N. Sato, and S. Isa, 1983: Description of the JMA operational spectral model. *J. Meteor. Soc. Japan,* **61,** 812–828.

Kitade, T., 1983: Nonlinear normal mode initialization with physics. *Mon. Wea. Rev.,* **111,** 2194–2213.

Krishnamurti, T. N., and H. S. Bedi, 1988: Cumulus parameterization and rainfall rates III. *Mon. Wea. Rev.,* **116,** 583–599.

——, J. Xue, H. S. Bedi, and D. Oosterhof, 1991: Physical initialization for numerical weather prediction over the tropics. *Tellus,* **43AB,** 51–81.

Lacis, A. A., and J. E. Hansen, 1974: A parameterization for the absorption of solar radiation in the earth's atmosphere. *J. Atmos. Sci.,* **31,** 118–133.

Lander, M. A., 1999: A tropical cyclone with a very large eye. *Mon. Wea. Rev.,* **127,** 137–142.

Louis, J. F., 1979: A parametric model of the vertical eddy fluxes in the atmosphere. *Bound.-Layer Meteor.,* **17,** 187–202.

Martin, J. D., and W. M. Gray, 1993: Tropical cyclone observation and forecasting with and without aircraft reconnaissance. *Wea. Forecasting,* **8,** 519–532.

Molteni, F., R. Buizza, T. N. Palmer, and T. Petroliagis, 1996: The ECMWF Ensemble Prediction System: Methodology and validation. *Quart. J. Roy. Meteor. Soc.,* **122,** 73–119.

Raj, R., 1998: Hydrological aspects of tropical cyclones. *WMO Bull.,* **47,** 345–354.

Robert, A. J., J. Henderson, and C. Turnbull, 1972: An implicit time integration scheme for baroclinic models of the atmosphere. *Mon. Wea. Rev.,* **100,** 329–335.

Sigrest, A. A., and R. Krzysztofowicz, 1998: Spatially averaged versus point precipitation in Monongahela Basin: Statistical distinctions for forecasting. *Wea. Forecasting,* **13,** 1063–1077.

Sivillo, J. K., and J. E. Ahlquist, 1997: An ensemble forecasting primer. *Wea. Forecasting,* **12,** 809–818.

Slingo, J., 1985: Cloud cover experimentation with the ECMWF model. *Proc. ECMWF Workshop on Cloud Cover Parameterization in Numerical Models,* Reading, United Kingdom, ECMWF, 163–212.

Tibbetts, R. T., 1999: An intercomparison of hurricane forecasts using SSM/I and TRMM rain rate algorithm(s). Ph.D. dissertation, The Florida State University, 126 pp.

Tiedtke, M., W. A. Heckley, and J. Slingo, 1988: Tropical forecasting at ECMWF: On the influence of physical parameterization on the mean structure of forecasts and analyses. *Quart. J. Roy. Meteor. Soc.,* **114,** 639–664.

Toth, Z., and E. Kalnay, 1997: Ensemble forecasting at NCEP and the breeding method. *Mon. Wea. Rev.,* **125,** 3297–3319.

Wallace, J. M., S. Tibaldi, and A. J. Simmons, 1983: Reduction of systematic forecast errors in the ECMWF model through the introduction of envelope orography. *Quart. J. Roy. Meteor. Soc.,* **109,** 683–718.

Zhang, Z., 1997: Hurricane ensemble prediction using EOF-based perturbations. Ph.D. dissertation, The Florida State University, 174 pp.

——, and T. N. Krishnamurti, 1997: Ensemble forecasting of hurricane tracks. *Bull. Amer. Meteor. Soc.,* **78,** 2785–2795.

——, and ——, 1999: A perturbation method for hurricane ensemble predictions. *Mon. Wea. Rev.,* **127,** 447–469.